Available at www.sciencedirect.com

ScienceDirect

journal homepage: www.elsevier.com/locate/he

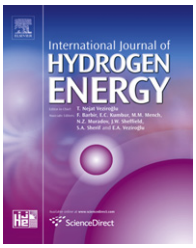

Anode-supported micro-tubular SOFCs fabricated by a phase-inversion and dip-coating process

Changcheng Chen [a,b,1], *Mingfei Liu* [a,1], *Lei Yang* [a], *Meilin Liu* [a,*]

[a] *Center for Innovative Fuel Cell and Battery Technologies, School of Materials Science and Engineering, Georgia Institute of Technology, 771 Ferst Drive, N.W., Atlanta, GA 30332, USA*

[b] *School of Physical Science and Technology, Lanzhou University, Lanzhou 730000, Gansu, People's Republic of China*

ARTICLE INFO

Article history:
Received 25 November 2010
Received in revised form
2 February 2011
Accepted 3 February 2011
Available online 9 March 2011

Keywords:
Micro-tubular SOFCs
Phase-inversion
Dip-coating
Anode-supported cell

ABSTRACT

A simple phase-inversion process is successfully combined with a dip-coating process to fabricate anode-supported micro-tubular solid oxide fuel cells (SOFCs). Several processing parameters were systematically investigated to optimize cell microstructure and performance, including the amount of pore former used in the support substrate and the number of electrolyte coatings. Single cells with ~240 μm thick NiO-YSZ support and 10 μm thick YSZ electrolyte were successfully fabricated, demonstrating peak power densities of 752 and 277 mW cm^{-2} at 800 and 600 °C, respectively, when a composite cathode consisting of $La_{0.85}Sr_{0.15}MnO_3$ and $Sm_{0.2}Ce_{0.8}O_{2-\delta}$ was used. This simple fabrication technique can be readily used for optimization of fuel cell microstructures and for cost-effective fabrication of high-performance SOFCs, potentially reducing the cost of SOFC technologies.

1. Introduction

Solid oxide fuel cells (SOFCs) are prospective next-generation energy conversion systems because of their high energy efficiency and excellent fuel flexibility [1–10]. The design of cell architecture and electrode microstructure may greatly influence the performance and reliability of SOFC systems. The advantages of tubular over planar SOFC systems include higher mechanical integrity, better thermal-cycling behavior and simpler gas manifolding and sealing [11–15]. In particular, small-sized tubular SOFCs, such as micro-tubular SOFCs (MT-SOFCs), hold the promise for improved thermo-mechanical stability, rapid start-up, high thermo-cycling resistance, and high volumetric power density [16–19]. Further, micro-tubular cells have the potential to reduce material cost by reducing cell weight [20].

The most common technique for fabrication of MT-SOFCs is the traditional extrusion method, which has the potential to be a cost-effective process with high reproducibility [20,21]. For laboratory investigations into the effect of cell architecture and electrode microstructure on performance, however, extrusion is equipment intensive and has long lead time for processing parameter adjustment. The extruded micro-tubular cells often show large internal resistance and relatively low performance [21]. For example, the peak power density for extruded flatted-tube cells at 850 °C was only ~550 mW cm^{-2} [15], even when the extruded surface of the NiO-YSZ anode supports were modified by a slurry coating of fine NiO-YSZ particles to tailor the surface roughness and the pore size whereas the cathodes were composed of three consecutive layers of a YSZ/LSM composite, a lanthanum strontium manganite (LSM), and an $La_{0.6}Sr_{0.4}Co_{0.2}Fe_{0.8}O_3$

* *Corresponding author*. Tel.: +1 404 894 6114; fax: +1 404 894 9140.
E-mail address: meilin.liu@mse.gatech.edu (M. Liu).

[1] These authors contributed equally to this work.

0360-3199/$ – see front matter
doi:10.1016/j.ijhydene.2011.02.016

(LSCF) layer to optimize the cathode performance. Recently, a phase-inversion technique has been introduced for fabrication of ceramic hollow fiber membranes, providing a rapid fabrication process for better control of the microstructure [16–18]. Although fiber membranes with a thin wall thickness and an asymmetric structure were fabricated using this method, a specially designed spinneret was required for shaping. Furthermore, it is noted that the power densities of the MT-SOFCs produced are much lower than the anticipated values. For example, the MT-SOFCs with a configuration of Ni-YSZ/YSZ/LSM-YSZ, fabricated using a phase inversion and a vacuum assisted coating process, demonstrated a peak power density of only 377 mW cm^{-2} at 800 °C [16].

In this article, we reported our findings in fabrication of anode-supported SOFCs with well controlled microstructures using a simple phase-inversion with dip-coating process. The effect of dip-coating on anode support thickness and the amount of pore former on the porosity and electrical conductivity of the anode supports were systematically studied. Furthermore, anode-supported full cells were fabricated and their electrochemical performances were evaluated under practical fuel cell operating conditions.

2. Experimental

2.1. Materials

Commercially available NiO (Alfa, USA) and 8 mol% yttria-stabilized zirconia (8YSZ, Daiichi-kigenso Co., Ltd) powders were used as the anode materials. Polyethersulfone (PESf) ((Radel A-300), Ameco Performance, USA), *N*-methyl-2-pyrrolidone (NMP) (HPLC Grade, 99.5%, Alfa, USA) and Polyvinylpyrrolidone (PVP) (Alfa, USA, M.W. = 8000) were used as polymer binder, solvent, and dispersant, respectively. Rice starch (Alfa, USA) was used as pore former to tailor the anode porosity. $La_{0.85}Sr_{0.15}MnO_3$ (LSM, Rhodia Inc. USA) and $Sm_{0.2}Ce_{0.8}O_{2-\delta}$ (SDC) powders were used as the cathode materials. The SDC powders were synthesized by a GNP method as described elsewhere [5].

2.2. Preparation of NiO-YSZ anode-supported cells

The tubular anode substrate was fabricated via a phase-inversion method [17]. Calculated amount of PESf and PVP was dissolved into the NMP to form a stable polymer solution. NiO and YSZ in a weight ratio of 55:45 with proper amount of rice starch (pore former) were dispersed in the solution, followed by ball-milled for 48 h using YSZ ball media to get a uniform and stable suspension. This suspension was then transferred to a vessel and degassed at room temperature under vacuum of $\sim 1 \times 10^{-1}$ bar for 30 min. The outer side of a one-end-closed steel tube was then dipped in the ceramic suspension to form a layer of NiO-YSZ, which was subsequently immersed in de-ionized water (coagulant agent) for 30 min to allow for an exchange between the water molecules and spinning solution molecules to take place. The dip-coating and phase-inversion process was repeated several times to obtain the desired thickness of the tubular anode support. After dried in air, the tubes were fired at 1100 °C for 2 h to obtain adequate mechanical strength for further application of electrolyte and cathode layers. The pre-fired tubes were dipped into YSZ suspension to form a YSZ electrolyte layer, which was then co-sintered at 1400 °C for 3 h to form a dense electrolyte membrane supported by the anode [22]. A slurry containing LSM and SDC powders (at a weight ratio of 7:3) was then brush painted on the YSZ electrolyte, followed by firing at 1150 °C for 2 h to form a porous LSM-SDC composite cathode. The resulting anode-supported MT-SOFCs have a typical length of ~3.0 cm, an outside/inside diameter of ~2.0 mm/1.5 mm, and an effective cathode area of ~1.0 cm^2.

2.3. Characterization methods

2.3.1. Microstructure and porosity of the tubes

Microstructures of the anode-supported MT-SOFCs were examined using a scanning electron microscope (SEM, LEO 1530). The porosity of the sintered NiO-YSZ anodes (at 1400 °C for 3 h) before and after reduction was measured using the Archimedes method.

2.3.2. Conductivity

The effective conductivity of the Ni-YSZ anodes was measured using a four-probe DC method. The voltages between the two inner probes were recorded when a current in the range of 0–10 mA was drawn from the two outer electrodes at a ramping rate of 0.02 mA/s. Linear fits to the *I*–*V* curves were used to determine the resistances of the anode substrates. The effective bulk conductivity of the anodes was calculated from the measured resistance and the sample geometry as follows:

$$\sigma_{anode} = \frac{L_{anode}}{R_{anode} A_{anode}} \quad (1)$$

where L_{anode} is the distance between the potential probes and A_{anode} is the cross-sectional area of the anode sample, which is given by:

$$A_{anode} = \frac{\pi}{4}(D_0^2 - D_i^2) \quad (2)$$

2.3.3. Electrochemical performance

The single tubular cells were sealed on ceramic support tubes with silver paste. Humidified hydrogen (~3%H_2O) at a flow rate of 30 sccm and stationary air were used as fuel and oxidant, respectively. The *I*–*V* curves and power outputs of test cells were monitored using an Arbin fuel cell testing system (MSTAT). Impedance spectra were acquired using a Solartron 1255 HF frequency response analyzer, interfaced with an EG&G PAR potentiostat model 273A. The frequency of the impedance measurement ranged from 100 kHz to 0.1 Hz and the AC amplitude was 5 mV.

3. Results and discussion

3.1. Microstructure of anodes with different dip-coating times

Fig. 1(a) shows the photograph of the micro-tubular SOFCs. Well-shaped cells with good quality were successfully fabricated by the phase-inversion and dip-coating method. This

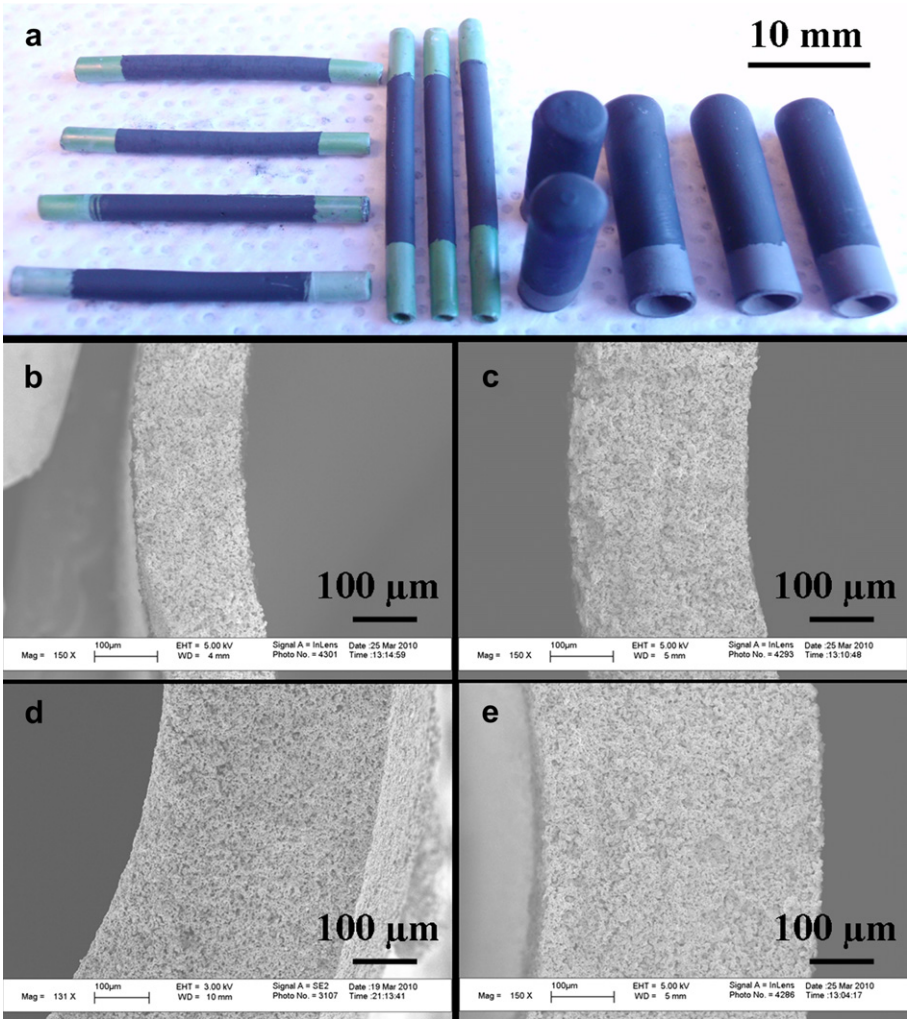

Fig. 1 – (a) Photographs of Ni-YSZ/YSZ/LSM-SDC tubular SOFCs, (b–e) cross-sectional views (SEM images) of Ni-YSZ anodes formed by multiple dip-coating: (b) once; (c) twice; (d) three times; and (e) four times.

process can also be used to fabricate hollow and one-end-closed tubes with different lengths and diameters. The one-end-closed tubular SOFCs are ~4.0 cm in length, outside/inside diameter of ~6.0 mm/4.0 mm, and an effective cathode area of ~5.5 cm^2. The anode thickness can be readily controlled by the number of dip-coatings. Shown in Fig. 1(b)–(e) are the SEM images for Ni-YSZ tubes with varying numbers of dip-coating (the tubes have been reduced under hydrogen at 800 °C). As shown in Fig. 2, the thickness of the Ni-YSZ anodes increased linearly with the number of dip coatings. On the other hand, the anodes have uniform sponge-like porous microstructures with typical pore size in the range of a few microns, and the tubes are free of cracks or other visible defects. The anode microstructures obtained in this study appear to be different from those reported in the literature [16–18,23]; the large finger-like pores formed during the phase-inversion process of previous studies are minimized or eliminated in this study. According to other reports, both the precipitation time and polyethersulfone concentration will influence the microstructure [24]. The uniform microstructure in our anode appreciably increases the grain connection and gas transport while maintaining adequate mechanical strength.

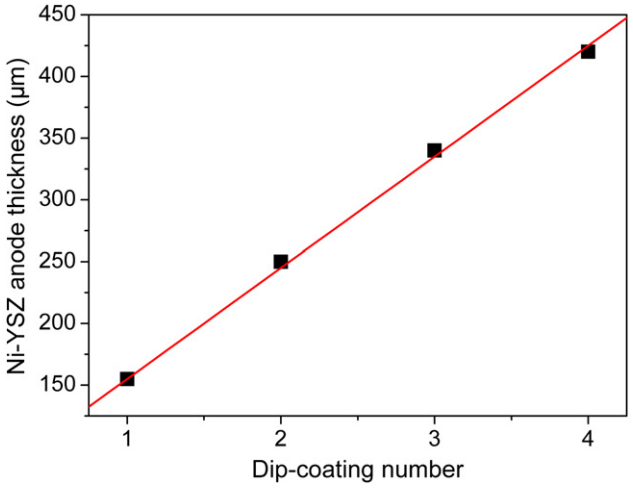

Fig. 2 – Ni-YSZ anode thickness as a function of dip-coating time.

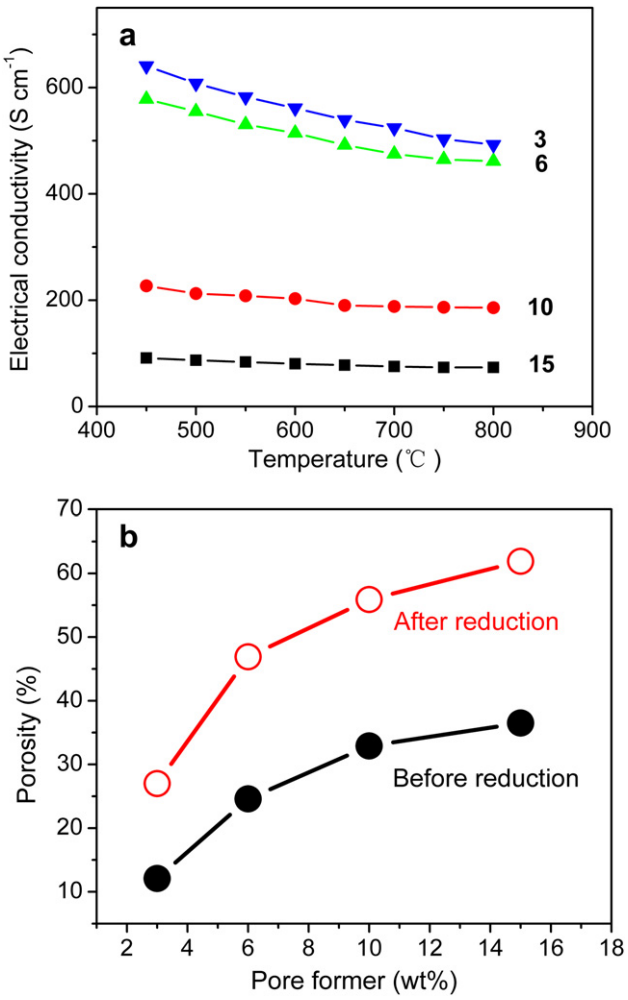

Fig. 3 – (a) The conductivities of Ni-YSZ anodes measured in dry hydrogen at different temperatures as a function of the content of pore former. The number by each set of data represents the amount of pore former (in weight %) added to the anode slurry. (b) The porosity of Ni-YSZ anodes before and after reduction in dry hydrogen.

3.2. *Effect of porosity on the electrical conductivity*

In general, electrodes should have sufficient porosity for rapid gas transport as well as adequate electrical conductance for current collection. For the tubular cells, the electrons have a longer path in the anode tube, which might contribute to the Ohmic resistance loss [20]. The conductivities for the as-prepared Ni-YSZ anode tubes under hydrogen are shown in Fig. 3(a). Each of the samples shows a typically metallic behavior. At a given temperature, the samples with lower pore former content show higher conductivity but lower porosity. As expected, the highest conductivity (i.e., 641 S cm^{-1} at 450 °C) was achieved in the sample containing 3 wt.% pore former while the porosity was ~27.0%. (The high conductivity is due to the higher metallic Ni volume content, because the conductivity of Ni is five orders of magnitude higher than that of YSZ) [17]. When the pore former was increased to 6 wt.%, the porosity of the anode was increased to ~46.9%, while the conductivity was reduced to ~578–462 S cm^{-1} in the temperature range studied. The conductivity as well as the porosity is high enough to meet the anode support SOFCs requirement. Further increase in pore former content to 10 and 15 wt.% significantly reduced the conductivities (at 450 °C) to ~227 and 91 S cm^{-1}, respectively.

Based on the above results, the anode with 6 wt.% of rice starch as pore former was selected for preparation of the required anode support for further electrochemical performance study. It should be noted that the porosity increased after reduction due to the reduction from NiO to Ni, as shown in Fig. 3(b).

3.3. *Microstructure of MT-SOFCs*

Fig. 4 shows the overall microstructure of an anode-supported MT-SOFC with ~240 μm anode, ~10 μm electrolyte, and ~20 μm cathode. Fig. 4(b) shows that the interfaces between the electrolyte and the electrodes are very coherent. The interfaces show no observable delaminations or cracks. In addition, the electrolyte layer is very dense without any cracks or other visible defects. Fig. 4(c) shows the microstructure of

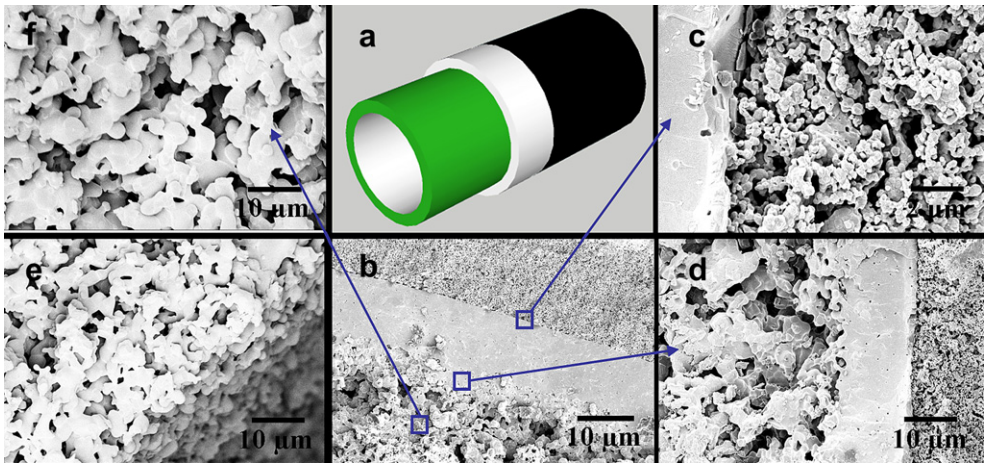

Fig. 4 – Schematic view (a) and cross-sectional views (SEM images) of an anode-supported MT-SOFC: (b) the whole cell, (c) the electrolyte/cathode interface; (d) the anode/electrolyte interface; (e) anode inner layer; (f) anode after reduction.

the cathode layer. After firing at 1150 °C for 2 h, continuous and uniform pores are left in the LSM-SDC matrix. Fig. 4(d) shows the porous anode layer close to the electrolyte with small sponge-like pores, which is considered to be the functional layer of the anode where electrochemical reactions take place. Furthermore, the small sponge-like pores adjacent to the electrolyte layer allow the YSZ particles to penetrate into the Ni-YSZ functional layer during the YSZ electrolyte film is prepared by dip-coating. It is expected that optimization of the anode-electrolyte interface microstructure will decrease the anode polarization by increasing the three phase boundaries (TPBs) length, as to be discussed later.

Fig. 4(e) shows that the anode inner layer is porous, containing uniform pores on the surface. Therefore, the anode layer is a good porous support, allowing fast gas transport. Fig. 4(f) shows the anode microstructure after reduction, consisting of Ni and YSZ. The phase-inversion and sintering produced desired anode microstructures, with a uniform distribution of Ni and YSZ grains, without cracks and providing a uniform distribution of TPBs in the anode. This uniform sponge-like porous structure of the anode is especially suitable for use as a support in MT-SOFCs because the larger pores may provide a path with negligible resistance to rapid gas transport while the smaller pores provide a large number of TPBs for the electrochemical reactions.

3.4. *Cell performances*

Fig. 5 shows the typical performance of an anode-supported MT-SOFC tested at 500–800 °C, demonstrating peak power densities of 105, 180, 277, 395, 522, 646, and 752 mW cm^{-2} at 500, 550, 600, 650, 700, 750, and 800 °C, respectively, when hydrogen was used as fuel and ambient air as oxidant. The open circuit voltage (OCV) varied from 1.09 to 1.04 V as the temperature was increased from 500 to 800 °C, close to the theoretical value calculated from the Nernst equation. The high OCV values indicate that the gas leakage through the electrolyte was negligible and the prepared electrolyte is very dense without any open cracks or pinholes. These demonstrated power densities are about twice of those previously reported for similar cells (12 μm YSZ electrolyte) fabricated by a phase inversion and vacuum assisted coating technique [16]. At 600 °C without catalyst impregnation, for example, the peak power density of our cells is ~277 mW cm^{-2} whereas that of the cells fabricated by similar procedures was only ~124 mW cm^{-2} [16]. The high performance at intermediate temperatures achieved in this work is attributed primarily to the optimization of the anode microstructure (proper porosity and electrical conductivity) and better control of the interfaces between the electrolyte and the anode support. It is noted that micro-tubular cells based on a complex tri-layer of electrolyte, $La_{0.6}Sr_{0.4}Co_{0.2}Fe_{0.8}O_{3-y}$-GDC cathode, and Ni-GDC anode demonstrated a peak power density of only 162 mW cm^{-2} at 550 °C [25]. The tri-layer of electrolyte consists of one layer of Sc_2O_3-stabilized ZrO_2 (ScSZ) sandwiched between two layers of Gd_2O_3-doped CeO_2 (GDC), which were fabricated using a multiple dip-coating (on a NiO-GDC supporting tube) and

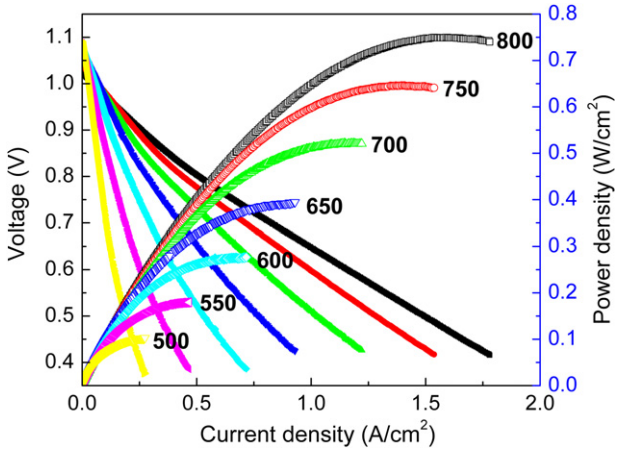

Fig. 5 – Typical current-voltage characteristics and the corresponding power densities for MT-SOFCs measured at 500–800 °C when ambient air was used as oxidant and hydrogen as fuel. The number by each set of data represents the temperature in °C at which the full cell performance was measured.

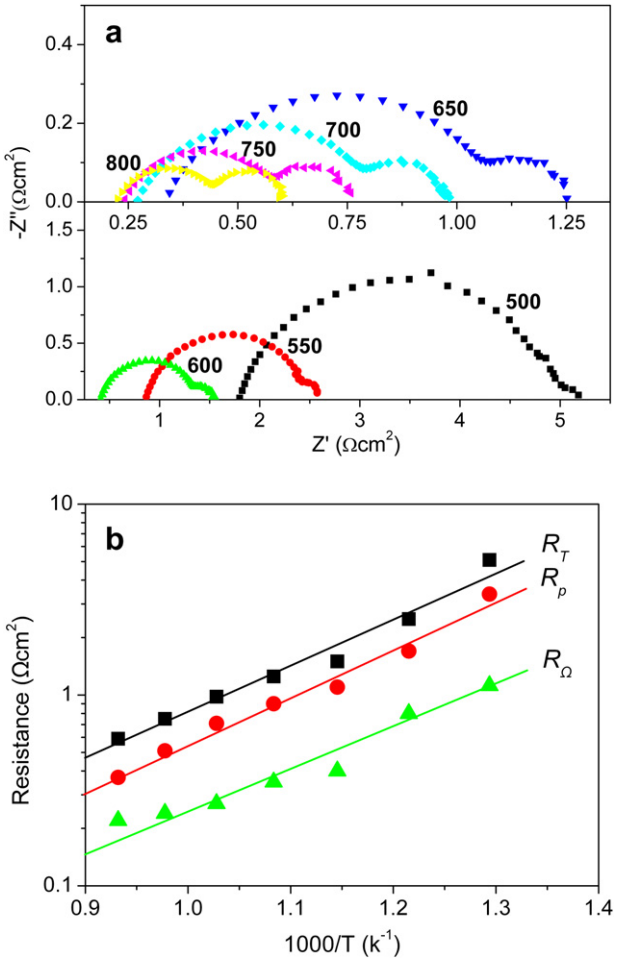

Fig. 6 – (a) Impedance spectra for MT-SOFCs measured under OCV conditions at 500–800 °C while running on hydrogen at flow rate of 30 sccm. The number by each set of data represents the temperature in °C at which the impedance was measured. (b) The total, interfacial polarization, and Ohmic resistance (R_T, R_p and R_Ω, respectively) of the MT-SOFC.

a co-firing process. It is also noted that the power densities of our cells (without catalyst impregnation) are close to those of micro-tubular cells with catalyst infiltration (with a cell configuration of Ni-SDC-YSZ/YSZ/LSM-YSZ-SDC) [17].

Fig. 6(a) shows impedance spectra for the anode-supported MT-SOFCs measured under OCV conditions. The total cell resistance was reduced from 5.10 to 0.59 Ω cm^2 while the Ohmic resistance was decreased from 1.72 to 0.22 Ω cm^2 when the temperature is increased from 500 to 800 °C. As expected, both the Ohmic loss and the polarization decreased with increasing temperature, due to the increased ionic conductivity of the electrolyte and faster electrode kinetics.

Fig. 6(b) shows the total resistance (R_T), interfacial polarization resistance (R_p) and Ohmic resistance (R_Ω) of the cell. The intercepts of the impedance arcs on the real axis at high frequencies correspond to the Ohmic resistance, which mainly comes from the electrolyte and lead wires, while the overall size of the impedance loop is attributed to the polarization resistance. These resistances are lower than those observed in previous studies using the phase-inversion method to fabricate MT-SOFCs (the total cell resistance was ~1.0 Ω cm^2 with R_Ω of ~0.75 and R_p of ~0.25 Ω cm^2 at 800 °C) [16]. The reduced cell resistance in this study is attributed to the improved electrode/electrolyte contact and improved electrode microstructure. For example, the interfacial polarization resistance at intermediate temperatures (e.g., 1.05 Ω cm^2 at 600 °C) is much lower than those reported for similar cells fabricated by a phase-inversion method (e.g., ~3.5 Ω cm^2 at 600 °C) [16]. This significant reduction in polarization resistance is attributed primarily to the desired microstructure of the anode-electrolyte interface, as seen in Fig. 4(d). Since the activation energy for ionic conductivity of the electrolyte is usually smaller than that for electrode polarization, the power output of tubular anode-supported SOFCs is more limited by interfacial resistances, more so at lower operating temperatures.

4. Conclusions

Anode-supported MT-SOFCs have been successfully fabricated using a phase-inversion and a dip-coating process. The thickness of the anode supports can be readily tailored by the number of dip-coatings whereas the porosity and conductivity of the anode supports can be controlled by the amount of pore former used. A porosity of 46.9% was obtained when 6 wt.% starch was used as pore former, resulting electrical conductivity of 578–462 S cm^{-1} at 450–800 °C. The electrochemical performance was evaluated in a single cell with a configuration of ~240 μm Ni-YSZ|10 μm YSZ|20 μm LSM-SDC. Peak power density reached 752 and 277 mW cm^{-2} at 800 and 600 °C, respectively, indicating that the anode-supported MT-SOFCs have a good potential for practical applications.

Acknowledgments

This material is based upon work supported as part of the Heterogeneous Functional Materials (HetroFoaM) Center, an Energy Frontier Research Center funded by the U.S. Department of Energy, Office of Science, Office of Basic Energy Sciences under Award Number DE-SC0001061. ML would like to acknowledge the partial support by the WCU Program administrated by UNIST.

REFERENCES

[1] Wang YZ, Yoshiba F, Kawase M, Watanabe T. Performance and effective kinetic models of methane steam reforming over Ni/YSZ anode of planar SOFC. Int J Hydrogen Energy 2009;34:3885–93.
[2] Zhan ZL, Barnett SA. An octane-fueled solid oxide fuel cell. Science 2005;308:844–7.
[3] Basu RN, Sharma AD, Dutta A, Mukhopadhyay J. Processing of high-performance anode-supported planar solid oxide fuel cell. Int J Hydrogen Energy 2008;33:5748–54.
[4] Steele BCH, Heinzel A. Materials for fuel-cell technologies. Nature 2001;414:345–52.
[5] Yang L, Wang SZ, Blinn K, Liu MF, Liu Z, Cheng Z, et al. Enhanced sulfur and coking tolerance of a mixed ion conductor for SOFCs:$BaZr_{0.1}Ce_{0.7}Y_{0.2-x}Yb_xO_{3-\delta}$. Science 2009; 326:126–9.
[6] Leng YJ, Chan SH, Khor KA, Jiang SP. Performance evaluation of anode-supported solid oxide fuel cells with thin film YSZ electrolyte. Int J Hydrogen Energy 2004;29:1025–33.
[7] Zhang SQ, Bi L, Zhang L, Yang CL, Wang HQ, Liu W. Fabrication of cathode supported solid oxide fuel cell by multi-layer tape casting and co-firing method. Int J Hydrogen Energy 2009;34:7789–94.
[8] Zuo CD, Zha SW, Liu ML, Hatano M, Uchiyama M. $Ba(Zr_{0.1}Ce_{0.7}Y_{0.2})O_{3-\delta}$ as an electrolyte for low-temperature solid-oxide fuel cells. Adv Mater 2006;18:3318–20.
[9] Yang L, Zuo CD, Wang SZ, Cheng Z, Liu ML. A novel composite cathode for low-temperature SOFCs based on oxide proton conductors. Adv Mater 2008;20:3280–3.
[10] Fu XZ, Melnik J, Low QX, Luo JL, Chuang KT, Sanger AR, et al. Surface modified Ni foam as current collector for syngas solid oxide fuel cells with perovskite anode catalyst. Int J Hydrogen Energy 2010;35:11180–7.
[11] Bai YH, Liu J, Wang CL. Performance of cone-shaped tubular anode-supported segmented-in-series solid oxide fuel cell stack fabricated by dip coating technique. Int J Hydrogen Energy 2009;34:7311–5.
[12] Barzi YM, Ghassemi M, Hamedi MH. Numerical analysis of start-up operation of a tubular solid oxide fuel cell. Int J Hydrogen Energy 2009;34:2015–25.
[13] Li CX, Li CJ, Guo LJ. Performance of a Ni/Al_2O_3 cermet-supported tubular solid oxide fuel cell operating with biomass-based syngas through supercritical water. Int J Hydrogen Energy 2010;35:2904–8.
[14] Suzuki T, Hasan Z, Funahashi Y, Yamaguchi T, Fujishiro Y, Awano M. Impact of anode microstructure on solid oxide fuel cells. Science 2009;325:852–5.
[15] Kim SD, Hyun SH, Moon J, Kim JH, Song RH. Fabrication and characterization of anode-supported electrolyte thin films for intermediate temperature solid oxide fuel cells. J Power Sources 2005;139:67–72.
[16] Yang CL, Li W, Zhang SQ, Bi L, Peng RR, Chen CS, et al. Fabrication and characterization of an anode-supported hollow fiber SOFC. J Power Sources 2009;187:90–2.
[17] Yang CL, Jin C, Chen FL. Micro-tubular solid oxide fuel cells fabricated by phase-inversion method. Electrochem Commun 2010;12:657–60.
[18] Yang NT, Tan XY, Ma ZF. A phase inversion/sintering process to fabricate nickel/yttria-stabilized zirconia hollow fibers as the anode support for micro-tubular solid oxide fuel cells. J Power Sources 2008;183:14–9.

[19] Akhtar N, Decent SP, Kendall K. A parametric analysis of a micro-tubular, single-chamber solid oxide fuel cell (MT-SC-SOFC). Int J Hydrogen Energy 2011;36(1):765–72.
[20] Suzuki T, Funahashi Y, Hasan Z, Yamaguchi T, Fujishiro Y, Awano M. Fabrication of needle-type micro SOFCs for micro power devices. Electrochem Commun 2008;10:1563–6.
[21] Suzuki T, Yamaguchi T, Fujishiro Y, Awano M. Fabrication and characterization of micro tubular SOFCs for operation in the intermediate temperature. J Power Sources 2006;160: 73–7.
[22] Liu MF, Gao JF, Dong DH, Liu XQ, Meng GY. Comparative study on the performance of tubular and button cells with YSZ membrane fabricated by a refined particle suspension coating technique. Int J Hydrogen Energy 2010;35: 10489–94.
[23] Liu SM, Gavalas GR. Oxygen selective ceramic hollow fiber membranes. J Membr Sci 2005;246:103–8.
[24] Jin C, Yang CH, Chen FL. Effects on microstructure of NiO-YSZ anode support fabricated by phase-inversion method. J Membr Sci 2010;363:250–5.
[25] Suzuki T, Hasan Z, Funahashi Y, Yamaguchi T, Fujishiro Y, Awano M. Fabrication and characterization of microtubular SOFCs with multilayered electrolyte. Electrochem Solid St 2008;11:B87–90.